ACS OMEGA

http://pubs.acs.org/journal/acsodf

Article

Research on Resistance to Water Intoxication of $LaCoO_3$ Doped with Fe at B Sites

Cuihua Hao, Xuefeng Wang,* Shuangli Du, Cunbao Deng, and Huijie Hu

Cite This: *ACS Omega* 2023, 8, 28448−28455

Read Online

ACCESS | Metrics & More | Article Recommendations

ABSTRACT: In this paper, the methods of spin polarization density functional theory and vasp software package are used to simulate the adsorption of H_2O molecules on the surface of $LaCoO_3$ and $La_2CoFeO_6(001)$. It was found that when Fe was doped at B-sites, the adsorption energy changed from −3.7493 eV at CoO_2 to −2.5397 eV at $CoFeO_4$, which decreased by about 1/3. Meanwhile, the change of electric charge and the amount of electron transfer decreased overall. The results indicated that Fe doping could inhibit the adsorption of H_2O by perovskites and thus hinder the next toxic reaction. Therefore, this paper will lay a certain theoretical foundation for the study of perovskite anti-poisoning mechanism and provide a meaningful reference for further experimental research.

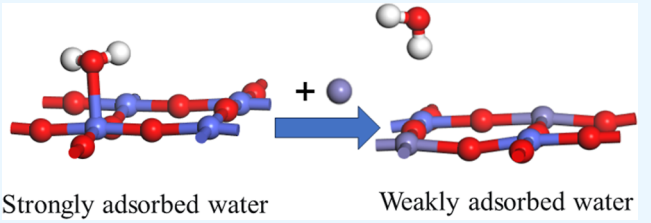

1. INTRODUCTION

Energy is the foundation and driving force for the progress of human civilization.[1] It is vital to national economy, people's livelihood, and national security and is crucial to promoting economic and social development and improving people's well-being.[2] Coal is the richest on the earth, the largest in the distribution of fossil fuels, China is a country with much coal and less oil, coal is in the absolute main position in our country's primary energy structure, accounting for more than 70%.[3] However, the ventilation air methane in coal mines can cause environmental pollution and global warming.[4−6] With the accelerated pace of the international community to cope with climate change and the establishment of China's double carbon target,[7,8] the utilization and treatment technology of exhaust gas has become a hot topic of scientific and technological workers.[9−11] The main component of the gas is methane, which can be burned at low temperatures to reduce the production of pollutants at the source.[12−14] At present, the catalysts used for methane catalytic combustion are mainly divided into non-precious metal catalysts and precious metal catalysts.[15,16] The non-precious metal catalysts are low in price, easy to obtain, and have strong thermal stability,[17] especially the high catalytic activity and thermal stability of perovskites, which has attracted wide attention.[18−20] In recent years, the $LaCoO_3$ perovskite plays a very important role in surface catalytic reactions and surface chemical reactions.[21]

However, poisoning of catalysts often occurs, which is mainly due to the strong interaction between toxic substances and active components and the destruction of the surface properties and structure of catalysts, leading to the reduction of their reactivity.[22] As a product of gas-catalyzed combustion reaction itself and an inevitable component in the actual environment, water vapor has an inhibitory effect on the catalytic process, but there is no clear theory. Generally, there are two viewpoints as follows: (1) H_2O will form competitive adsorption with CH_4. After occupying the active site, H_2O will easily form hydroxides and deactivate, but it will be decomposed into the corresponding active oxide components at high temperatures.[23] (2) H_2O is decomposed into the hydroxyl group on the catalyst surface, and the accumulation of a large amount of hydroxyl group on the catalyst surface prevents the activation of methane and oxygen on the catalyst surface.[24] The kinetic rate equation of methane oxidation measured by Li Xiansheng is as follows: $r = k(CH_4)^{0.7}(O_2)^{0.2}(H_2O)^{-0.9}$,[25] while the reaction order of water on the supported nano-palladium catalyst is 0.9−1.1.[26] Burch et al. observed that the inhibitory effect of water decreased with increasing temperature drop and was negligible above 450 °C.[27] Persson et al. investigated the methane catalytic combustion activity of $Pt−Pd/Al_2O_3$ cocatalysts with different Pt/Pd ratios at 500 °C and 5% H_2O and found that with the increase of Pt content, the inhibitory effect of H_2O on the catalytic activity decreased significantly. When the H_2O mixed in methane was removed, the activity of $Pt−Pd/Al_2O_3$ co-catalyst was higher than the initial activity, while the catalytic activity of Pd/Al_2O_3 decreased significantly.[28] Huang

Received: April 19, 2023
Accepted: July 12, 2023
Published: July 24, 2023

studied water in flue gas, so as to choose a new V_2O_5/AC catalyst for catalytic reduction of NO effects and found water to exhibit the competitive adsorption of reactants and, to a certain extent, reduces the activity of the catalyst; the removal of activated coke carrier minerals can slow the rate of catalyst deactivation to a certain degree but cannot completely inhibit water poisoning of the catalyst role.[29] Li et al. investigated the effect of adding H_2O to the reaction gas on the activity of Mo-based catalysts and found that adding water to the reaction gas could cause irreversible inactivation of the Mo-based catalyst supported by Al_2O_3, while adding C could protect the active component MoS_2 on the Mo-based catalyst and inhibit the irreversible inactivation caused by water.[30] The $M_xCe_{1-x}O_\delta$ /3DOM-mSiO_2 catalyst prepared by Yu et al. shows good catalytic combustion soot activity. Density functional theory (DFT), X-ray diffraction (XRD), and Raman prove that the catalyst poisoning is mainly due to the reaction of SO_2 adsorbed by the catalyst with reactive oxygen species and metal atoms to form sulfate species, leading to the reduction of catalytic activity.[31]

The above-related experiments have proved that the addition of iron to perovskites can reduce the effect of water poisoning of the catalyst and improve the efficiency of catalytic methane, but the relevant mechanism is still not mastered. Therefore, this paper will use chemical simulation calculations to obtain a La_2CoFeO_6 catalyst by doping Fe at the B position of $LaCoO_3$ through DFT and study the effect of the mechanism of Fe doping on the physicochemical properties of the catalyst and the mechanism of water poisoning in order to provide effective theoretical supports for the design and development of future perovskite catalysts.

2. COMPUTATIONAL METHODS AND MODELS

The calculations in this paper are based on DFT, mainly using Vienna Ab-initio Simulation Package (VASP) version 5.4.4,[32] supplemented by Materials studio software.[33] The commutative correlation potential is calculated using the projector augmented wave (PAW) pseudo-potential of the generalized gradient approximation method (GGA) proposed by Perdew–Burke–Ernzerhof (PBE), using a planar wave base group.[34−37] Making sure the structure relaxes sufficiently to reach the lowest energy value.

Parameter setting: truncation can take 520 eV, iterative convergence accuracy: EDIFF = 1×10^{-5} eV and EDIFFG = 1×10^{-4} eV. For *k*-point meshes, the more numerous the more accurate, but at the same time the amount of computation will be increased, preferably selecting $7 \times 7 \times 7$ as the *k*-point of the bulk phase, while the *k*-point of the surface is set to $7 \times 7 \times 1$. Considering the effects of spin polarization, ISPIN = 2.

The sections were conducted according to the perovskite $LaCoO_3$ and La_2CoFeO_6[38] models established in previous studies: the optimized unit cell is cut in the 001 direction, the cell is expanded, the number of atomic layers established is 7 layers, and in order to eliminate the interference of the interaction between the bottom layer and the top layer atoms, the vacuum layer thickness is a 15 Å model and is optimized, and the optimized structure of $LaCoO_3(001)$ and $La_2CoFeO_6(001)$ is shown in Figure 1.

The H_2O molecule was placed in the same lattice as the LaO terminal surface, with a truncation energy ENCUT = 520 eV, a *k* point of 1, and a PAW potential for pseudopotential. The O atom in H_2O is sp^3 hybridized, and the middle O forms two single bonds with the H on both sides. At the same time, there

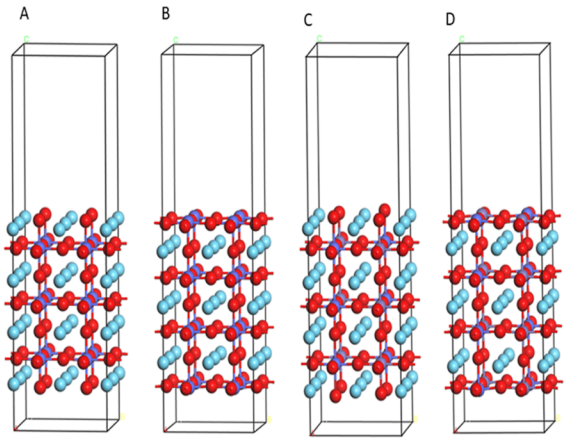

Figure 1. Configuration after optimization of $LaCoO_3$ and La_2CoFeO_6 finales. (A) LaO finales of $LaCoO_3$, (B) CoO_2 finales of $LaCoO_3$, (C) LaO finales of La_2CoFeO_6, and (D) $CoFeO_4$ finales of La_2CoFeO_6.

are two lone pair electrons left, and the lone pair electrons repel each other so that the single bond gathers in the middle, forming the V-shape. After optimization, the total energy of H_2O is −14.2067 eV, the bond length is 0.972 A, and the bond angle is 104.626°. The optimized structure is shown in Figure 2.

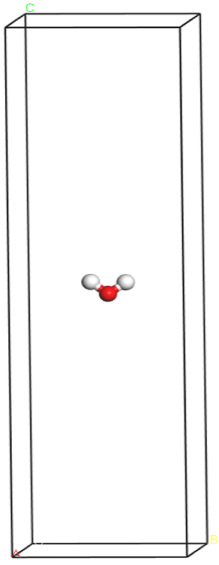

Figure 2. Optimized H_2O molecular model diagram.

3. RESULTS AND DISCUSSION

3.1. Adsorption Energy. H_2O molecules in the initial conformation, H down and O down, are on the LaO end surface of $LaCoO_3$ with two adsorption sites La and O and CoO_2 with two adsorption sites Co and O on the end surface of $LaCoO_3$. Adsorption of La and O is on the LaO terminal surface of La_2CoFeO_6 and Co, Fe, and O on the terminal surface of $CoFeO_4$.

The calculation formula for adsorption energy is as follows

$$E_{abs} = E_{(H_2O+slab)} - E_{H_2O} - E_{slab}$$

https://doi.org/10.1021/acsomega.3c02686
ACS Omega 2023, 8, 28448−28455

Among them: $E_{(H_2O+slab)}$ is the energy of the system when there is an adsorbent and E_{H_2O} is the energy of the adsorbent. E_{slab} is the energy of the surface when there is no adsorbent.

After H_2O optimization, $E_{H_2O} = -14.2067$ eV was calculated.

The total energies of the LaO termination surface and CoO_2 termination surface of $LaCoO_3$ and the LaO termination surface and $CoFeO_4$ termination surface of La_2CoFeO_6 are shown in Table 1.

Table 1. Total Energies of the LaO and CoO_2 Surfaces of $LaCoO_3$ and the LaO and $CoFeO_4$ Surfaces of La_2CoFeO_6

slab	$LaCoO_3$		La_2CoFeO_6	
	LaO-terminated	CoO_2-terminated	LaO-terminated	$CoFeO_4$-terminated
E/eV	−491.9469	−491.0587	−504.0109	−511.0606

Adsorption of H_2O on LaO(001) and CoO_2(001) termination surfaces of $LaCoO_3$: the calculated adsorption model is shown in Figure 3.

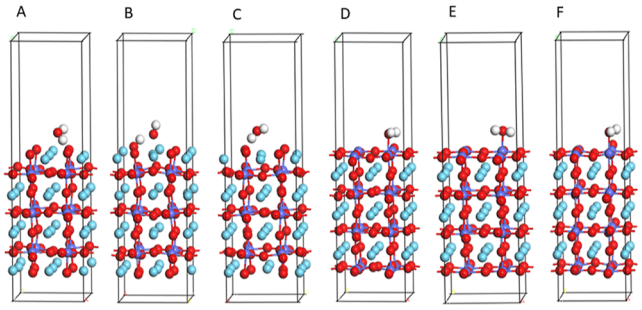

Figure 3. Structures of H_2O adsorption on LaO and CoO_2 termination surfaces of $LaCoO_3$. (A) H−La of LaO, (B) H−O of LaO, (C) O−La of LaO, (D) H−Co of CoO_2, (E) H−O of CoO_2, and (F) O−Co of CoO_2.

By observing the optimized adsorption model, it is found that the three initial configurations of H_2O adsorbed on the LaO(001) surface of $LaCoO_3$ are all optimized to be H downward adsorbed on O on the surface, the hydrogen−oxygen bond of H_2O molecules is elongated, and the distance between O in H_2O and LaO surfaces is shortened. The initial configuration for the H−O adsorption manner and hydroxyl hydrogen bond fracture is completely free of hydrogen, and free of hydrogen and oxygen combine to form on the surface of the new hydroxyl, the cycle, a large number of hydroxyl groups on the surface of the catalyst, accumulating prevented methane and oxygen in the catalyst surface activation, which coincide with water intoxication views 2. After optimization, the three initial configurations of H_2O attached to the CoO_2(001) surface of LaCoO3 are all O down and adsorbed to Co on the surface. Compared with the adsorption on the LaO surface, the hydrogen and oxygen bonds of H_2O molecules on the CoO_2 surface do not change significantly, and no hydroxyl group is formed, indicating that O on the LaO surface is more active and easier to adsorb H_2O molecules.

The results of adsorption energy, bond lengths, and bond angles of H_2O on LaO(001) and CoO_2(001) surfaces of LaCoO3 are shown in Table 2.

where E_{abs} is the adsorption energy, the positive value is endothermic, and the negative value is exothermic. The larger the absolute value is, the more heat is released, the larger the adsorption energy is, the more stable it is. Bond length refers to the bond length of O−H1 in H_2O molecules, where H1 refers to the nearest H to the surface and bond angle refers to the horizontal angle formed between H1 and the nearest metal atom on the surface. d is the distance from the proximal end of the H_2O molecule to the surface.

By comparison of adsorption energies, it is found that the adsorption energies of three adsorption configurations of H_2O on the LaO(001) surface are all greater than those on the CoO_2(001) surface, and H_2O is more likely to adsorb on the LaO surface. On the LaO surface, H_2O adsorbed at the top position of O with the initial configuration of H down has the maximum adsorption energy, which is −5.1139 eV, which is the most stable adsorption mode. On the contrary, H_2O adsorbed at the top position of La with H down has the lowest adsorption energy of −3.8113 eV, which is prone to desorption. However, the adsorption energy of H_2O adsorbed at the top position of La with O down is between the two. On the CoO_2 surface, H_2O adsorbed at the top position of Co and O in the initial configuration with H down and that adsorbed at the top position of Co with O down. These three ways were finally optimized to the top position of Co with O down. The adsorption energy difference between those was small. The maximum adsorption energy was 3.7493 eV, when H_2O was adsorbed at the top position of Co with O down, which proves that the top site of Co is the best adsorption site. By comparing the distance between H_2O and the surface, it is found that the distance between H_2O and LaO(001) surfaces is closer than that between the CoO_2(001) surface, and the greater the adsorption energy, the closer the distance to the surface is, which proves that the distance between the H_2O molecule and the surface is inversely proportional to the adsorption energy. Comparing the H−O bond lengths of H_2O molecules, it is found that the bond lengths of H_2O molecules adsorbed on the LaO surface are all greater than 1 A, while the bond lengths of H_2O molecules adsorbed on the CoO_2 surface are all less than 1 A. Moreover, the larger the adsorption energy, the longer the bond lengths, which proves that the H−O bond lengths of H_2O molecules are proportional to the size of the adsorption energy. The larger the adsorption energy, the more easily the H−O bond is elongated, and the more stable the O atoms adsorbed on the LaO surface. However, the bond angle has no

Table 2. Adsorption Energy, Bond Length, and Bond Angle of H_2O on LaO(001) and CoO_2(001) Surfaces of LaCoO3

	LaO-terminated			CoO_2-terminated		
	H−La	H−O	O−La	H−Co	H−O	O−Co
E_{abs}/eV	−3.8113	−5.1139	−4.7256	−3.5932	−3.6089	−3.7493
d/Å	1.242	0.908	1.374	2.144	2.074	1.888
length/Å	1.050	1.601	1.047	0.977	0.978	0.979
angle/deg	60.555	42.751	54.017	72.337	66.608	69.237

https://doi.org/10.1021/acsomega.3c02686
ACS Omega 2023, 8, 28448−28455

obvious law and is independent of the adsorption structure. In particular, when H_2O adsorbed at the top position of O on the LaO surface with a H down, the distance was the closest, which was much smaller than that of other adsorption methods (0.908 A), and the bond length at this time was the longest, which was longer than 1/2 of the bond length in other adsorption methods. This indicates that when H−O adsorbed, the H−O bond of H_2O was constantly stretched, and H of H_2O molecule was close to O on the LaO surface. Finally, the H−O bond of H_2O molecule near the surface is broken and divided into the hydroxyl group and free hydrogen, which in turn adsorbs with O on the surface to form a new hydroxyl group, leading to the accumulation of hydroxyl group on the LaO surface, occupying the adsorption site of methane and oxygen and further hindering the methane catalytic combustion reaction.

Adsorption of H_2O on LaO(001) and $CoFeO_4$(001) surfaces of La_2CoFeO_6: the calculated adsorption model is shown in Figure 4.

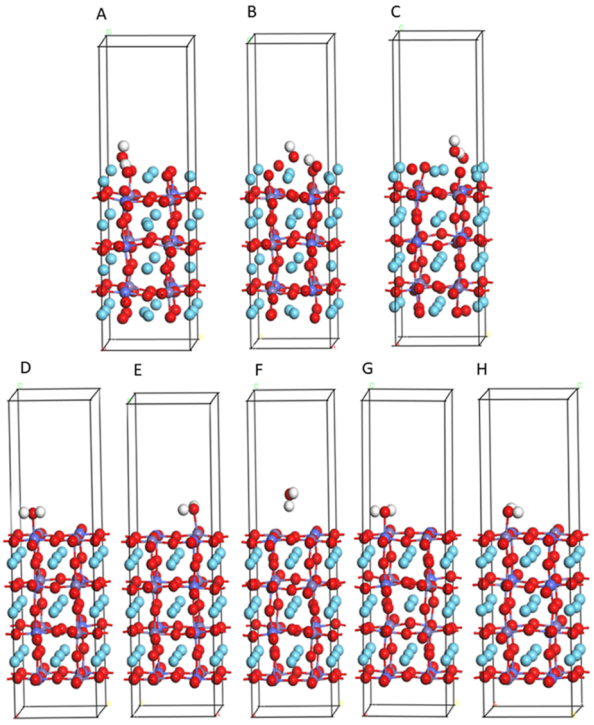

Figure 4. Adsorption model of H_2O on LaO and $CoFeO_4$ surfaces of La_2CoFeO_6. (A) H−O of LaO, (B) H−La of LaO, (C) O−La of LaO, (D) H−Co of $CoFeO_4$, (E) H−Fe of $CoFeO_4$, (F) H−O of $CoFeO_4$, (G) O−Co of $CoFeO_4$, and (H) O−Fe of $CoFeO_4$.

By observing the optimized adsorption model, it is found that the three initial configurations of H_2O adsorbed on the LaO(001) surface of La_2CoFeO_6 are similar to the LaO(001) surface of $LaCoO_3$, which are optimized to be H down and O adsorbed on the surface, and the H−O bond of H_2O molecules in the three initial adsorption configurations is stretched longer. The H atom in H_2O is closer to the O atom on the LaO surface, and the H−O bond of H_2O is completely broken and the free hydrogen combines with the oxygen on the surface to form a new hydroxyl group. The H−O adsorption is more intense, which proves that Fe doping in LaCoO3 will aggravate the poisoning on the LaO(001) surface. After optimization, the five initial configurations of H_2O attached to the $CoFeO_4$(001) surface of La_2CoFeO_6 changed to different degrees. Among them, H_2O molecules adsorbed with Co on the surface in the H direction down to the O direction down. The adsorption of Fe with H down on the surface changes to O down on the surface. The adsorption configurations of Co and Fe on the surface with O down were still the original ones. However, the initial configuration adsorbed to O on the surface with H down does not adsorb, which proves that the stable adsorption configuration on the surface of $CoFeO_4$(001) is that H_2O molecules adsorb to Co or Fe with O down. Different from the LaO(001) surface, H−O does not adsorb on the $CoFeO_4$ surface, which proves that the activity of O on these two surfaces is quite different when it adsorbs with the H_2O molecule.

The calculated results of adsorption energy, bond length, and bond angle are shown in Table3.

By comparison of adsorption energies, it is found that the adsorption energies of three adsorption configurations of H_2O on the LaO(001) surface are all greater than those on the $CoFeO_4$(001) surface. On the LaO surface, the adsorption energy is between −6 and −5 eV. On the surface of $CoFeO_4$, the adsorption energy is between −3 and −1. On the LaO surface, the adsorption energies of the three initial adsorption structures do not change significantly, which is related to the unified structure of H−O adsorption after optimization. Among them, H_2O adsorbed at the initial configuration of La with O down and changed to H down adsorbed at the top position of O with a maximum adsorption energy of −5.1139 eV, which is the most stable adsorption method. On the surface of $CoFeO_4$, the initial configuration of H_2O adsorbed on Fe with H down is optimized, and the maximum adsorption energy is −2.5397 eV when H_2O adsorbed on the top site of Fe with O down after optimization, which proves that the top site of Fe is the best adsorption site. Comparing the distance between H_2O and the surface, it is found that the distance between H_2O and the LaO(001) surface is about 0.5 A, while the distance between H_2O and the $CoFeO_4$(001) surface is more than 2 A, which further verifies that the distance between the H_2O molecule and the surface is inversely proportional to the adsorption energy. Comparing the H−O bond lengths of H_2O molecules, it is found that the bond lengths of H_2O molecules adsorbed on the LaO surface are all longer than 1.5 A. The H−O bond of H_2O molecules breaks and the free

Table 3. Adsorption Energy, Bond Length, and Bond Angle of H_2O on LaO and $CoFeO_4$ Surfaces of La_2CoFeO_6

	LaO-terminated				$CoFeO_4$-terminated			
	H−O	H−La	O−La	H−Co	H−Fe	H−O	O−Co	O−Fe
E_{abs}/eV	−5.1874	−5.3334	−6.0760	−2.031	−2.5397	−2.0356	−1.4322	−2.3780
d/Å	0.576	0.524	0.506	2.170	2.145	2.780	2.1435	2.1682
length/Å	1.569	1.627	1.620	0.974	0.979	0.974	0.978	0.979
angle/deg	48.944	58.475	56.074	71.068	83.147	58.777	66.706	62.768

https://doi.org/10.1021/acsomega.3c02686
ACS Omega 2023, 8, 28448−28455

hydrogen adsorbs with the O on the surface, forming a new hydroxyl group. However, on the $CoFeO_4$ surface, the bond length of H_2O molecules is less than 1A, which has little change from the bond length of free water molecules without adsorption (0.972 A). This proves that the H−O bond of H_2O molecules on the surface of $CoFeO_4(001)$ does not elongate or break significantly, and no new hydroxyl group is formed when the Fe element is doped with $LaCoO_3$. Furthermore, the accumulation of hydroxyl groups on the surface of $CoFeO_4$ is avoided, which prevents the further reaction of H_2O molecules on the surface. Therefore, Fe doping on the $CoFeO_4$ surface can effectively improve the water poisoning phenomenon in the methane-catalyzed reaction.

By comparing Tables 2 and 3, it can be seen that the most stable adsorption configuration of H_2O on the LaO surface of LaCoO3 is H−O adsorption with an adsorption energy of −5.1139 eV, and the most stable adsorption configuration on CoO_2 is O−Co adsorption with an adsorption energy of −3.7493 eV. However, the most stable adsorption configuration on the LaO surface is still H−O adsorption with an adsorption energy of −6.0760 eV, which increases by about 1/5. On the $CoFeO_4$ surface, the most stable adsorption configuration changes to O−Fe adsorption, and the best adsorption site changes from Co to the top site of Fe, which may be due to the fact that the magnetic properties of Fe are greater than that of Co. Conducive to the adsorption of H_2O molecules. The adsorption energy is −2.5397 eV, which decreases by about 1/3. However, the CoO_2 surface was doped with the Fe element before the calculation, while the LaO surface was not processed, indicating that the adsorption performance of the $CoFeO_4$ surface was reduced after Fe element doping, which made it difficult for H_2O molecules to adsorb on the $CoFeO_4$ surface, thus inhibiting the next chemical reaction. It is proved that Fe doping can effectively improve the water-poisoning resistance of LaCoO3 catalyst.

3.2. Bader Charge and Deformation Charge Density.

In order to explain the electron transfer before and after adsorption of H_2O molecule and understand the change law of electron transfer before and after $LaCoO_3$-doped Fe, the H_2O molecule is adsorbed on the LaO(001) terminal surface of $LaCoO_3$ by the H−O binding mode and $CoO_2(001)$ terminal surface by the O−Co binding mode. Moreover, the Bader charge analysis was carried out for the four most stable conditions, namely, the LaO(001) terminal surface adsorbed on La_2CoFeO_6 by the H−O binding mode and $CoFeO_4(001)$ terminal surface adsorbed on the O−Fe binding mode. The electron-transfer size and direction were judged by the gain and loss of atomic charges on the surface layer and the gain and loss of H_2O molecular charge. Moreover, by comparative analysis, the Bader charge of LaO(001) terminal surface of H_2O molecule adsorbed on LaCoO3 and $La_2CoFeO6$ by H−O binding is shown in Table 4. The Bader charges on the $CoO_2(001)$ surface of $LaCoO_3$ adsorbed by O−Co binding and $CoFeO_4(001)$ terminal surfaces of La_2CoFeO_6 adsorbed by O−Fe binding is shown in Table 5.

A positive value in the Bader charge table indicates that electrons are gained, and negative values indicate that electrons are lost; in the differential charge density chart, blue indicates the obtained electrons and yellow indicates the lost electrons.

In order to have a deeper understanding of the adsorption mechanism and bonding situation, the differential charge density map of these four adsorption methods is drawn, which can visually see the adsorption sites of molecules and the flow of electrons between H_2O molecules and the surface. H_2O molecules adsorbed on the LaO(001) terminal surface of $LaCoO_3$ and La_2CoFeO_6 in a H−O binding manner. The differential charge density diagrams of $CoO_2(001)$ surface adsorbed on $LaCoO_3$ by O−Co binding and $CoFeO_4(001)$ terminal surface adsorbed on La_2CoFeO_6 by O−Fe binding are shown in Figure 5.

Table 4. Bader Charge of LaO(001) Terminal Surface of H_2O Molecule Adsorbed on $LaCoO_3$ and La_2CoFeO_6 by H−O Binding

Bader	$LaCoO_3$			La_2CoFeO_6		
	LaO	LaO + H_2O	Δ	LaO	LaO + H_2O	Δ
La	9.0263	8.9581	−0.0682	9.0074	8.9917	−0.0157
	8.9720	8.9499	−0.0221	9.0119	8.9525	−0.0594
	9.0199	8.9561	−0.0638	8.9931	8.9564	−0.0367
	8.9681	8.9610	−0.0071	8.9911	8.9634	−0.0277
O	7.2461	7.2119	−0.0342	7.3191	7.3127	−0.0064
	7.3514	7.3947	0.0433	7.3345	7.3480	0.0135
	7.2989	7.2733	−0.0256	7.3395	7.4060	0.0665
	7.2652	7.2649	−0.0003	7.2705	7.2887	0.0182
O′	6.9711	7.3117	0.3406	6.9564	7.3462	0.3898
H	0.3965	0.4540	0.0575	0.3866	0.4062	0.0196
	0.6324	0.3538	−0.2786	0.6570	0.3397	−0.3173
H_2O	8	8.1195	0.1195	8	8.0921	0.0921

Yellow represents areas where charge density increases and blue represents areas where charge density decreases.

It can be seen from Table 4 and Figure 5 that, for the LaO-terminated face of LaCoO3, after adsorption of H_2O molecules, the charges of La atoms on the surface are reduced and electrons are lost, and the differential density map shows blue regions around La atoms, where the charges of La atoms closest to H_2O molecules decrease the most. For O atoms on the surface, the charge of O atoms on the LaO surface adsorb H_2O increases and electrons are obtained. Meanwhile, the differential density map shows that the yellow region is around O atoms, while the charge of O atoms on other surfaces decreases and the blue region is around them, and the area of yellow region is larger than that of the blue region. It is verified that the electrons gained by O atoms adsorbing H_2O molecules on the LaO surface are larger than the electrons lost by the other O atoms. The overall charge of H_2O molecule increases, in which the charge of O atoms and H atoms far away from the surface increases, while the charge of H atom adsorbed on the surface decreases. The differential charge density diagram also shows that one of the two H atoms in H_2O is surrounded by yellow, and the other is surrounded by blue. This indicates that when H_2O molecules adsorb, the charge on the LaO surface is transferred to H_2O molecules. For LaO-terminated faces of La_2CoFeO_6, similar to LaO-terminated faces of $LaCoO_3$, the La atomic charges on the surface are reduced, and the surrounding areas are blue. For the O atoms on the surface, the charges of other O atoms increase except for the O atoms far away from the H_2O molecule, and the O atoms adsorbing H_2O gain the most electrons and have a large yellow area around them. In H_2O molecules, the direction of electron transfer of H and O atoms is the same as in the LaO side of $LaCoO_3$ and H_2O molecules' whole electron transfer is reduced, but every atom of H_2O charge change quantity increased, proving that after $LaCoO_3$ doping with the Fe element, electron transfer increases,

https://doi.org/10.1021/acsomega.3c02686
ACS Omega 2023, 8, 28448−28455

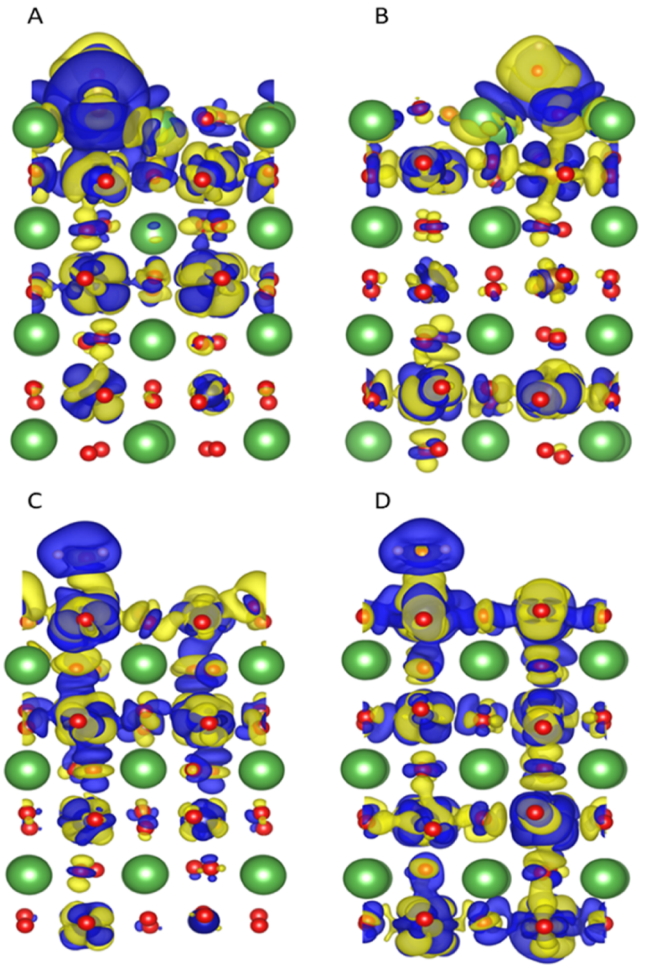

Figure 5. Differential charge density diagrams. (A) LaO of $LaCoO_3$ adsorbed by H_2O molecules in the H−O binding mode. (B) LaO of La_2CoFeO_6 adsorbed by H_2O molecules in the H−O binding mode. (C) CoO_2 of $LaCoO_3$ adsorbed by H_2O molecules in the H−O binding mode. (D) $CoFeO_4$ of La_2CoFeO_6 adsorbed by H_2O molecules in the H−O binding mode.

surrounded by a yellow and blue area, which correspond to adsorption increases. That is, the larger the adsorption energy, the more charge transfer, and the easier it is to adsorb H_2O molecules.

It can be seen from Table 5 and Figure 5 that for the CoO_2-terminated face of $LaCoO_3$, after adsorption of H_2O molecules, the Co atom charge on the surface increases and decreases, and the surrounding areas are yellow and blue, in which the Co atom that adsorbs H_2O is the largest electron transfer, surrounded by blue, the charge is reduced and electrons are lost. At the same time, Co near H_2O also loses electrons, while Co far away from H_2O has a little electron gain. For the O atoms on the surface, except for the two O atoms far away from H_2O, which have a little electron loss, the other six O atoms are all yellow, and the charge increases and the electrons are gained. The charge of the O atom in the H_2O molecule decreases, and the yellow color around the two H atoms increases, and the overall performance results in gaining electrons from the CoO_2 surface. For the $CoFeO_4$-terminated face of La_2CoFeO_6, the two Fe atoms are surrounded by blue, with reduced charge, and the Co atoms are surrounded by yellow, with increased charge, indicating that Fe is stronger in electron removal than Co. The charge of O atom increases and decreases, but the area of yellow and blue around it is smaller than that of Fe and Co atoms, and the electron transfer is smaller than that of Fe and Co atoms. The H_2O molecule is completely surrounded by blue, the charge amount of O and H atoms decreases, and the charge-transfer amount of H atom is greater than that of O, indicating that the electrons of H_2O molecule transfer to the surface of $CoFeO_4$ when the H_2O molecule is adsorbed. By comparing the Bader charges on the surface of CoO_2 and $CoFeO_4$, it is found that on the CoO_2 surface, electrons are mainly transferred from Co atoms on the surface to O in H_2O. After Fe doping, the electron transfer is changed from H and O in H_2O and from Fe atom to Co atom on the surface of $CoFeO_4$. In addition, after $LaCoO_3$ was doped with the Fe element, the overall charge change and electron transfer decreased, which also corresponded to the decrease of adsorption energy, that is, the adsorption ability of H_2O molecule on the $CoFeO_4$ surface was weakened after Fe

Table 5. Bader Charges on the CoO_2(001) Surface of $LaCoO_3$ Adsorbed by O−Co Binding and $CoFeO_4$(001) Terminal Surface of La_2CoFeO_6 Adsorbed by O−Fe Binding

Bader	$LaCoO_3$			Bader	La_2CoFeO_6		
	CoO_2	$CoO_2 + H_2O$	Δ		$CoFeO_4$	$CoFeO_4 + H_2O$	Δ
Co	7.5315	7.5520	0.0205	Fe	12.3573	12.2986	−0.0587
	7.6697	7.4835	−0.1862		12.3583	12.2899	−0.0684
	7.6997	7.6756	−0.0241	Co	7.5149	7.6101	0.0952
	7.5430	7.5448	0.0018		7.5258	7.6582	0.1324
O	7.0758	7.0880	0.0122	O	7.0760	7.0694	−0.0066
	7.1010	7.0875	−0.0135		7.1455	7.1357	−0.0098
	7.0694	7.0660	−0.0034		7.1414	7.1530	0.0116
	6.9751	6.9869	0.0118		7.1027	7.0895	−0.0132
	7.0390	7.0684	0.0294		7.1451	7.1393	−0.0058
	7.0045	7.0217	0.0172		7.0616	7.0698	0.0082
	7.0439	7.0526	0.0087		7.0960	7.0847	−0.0113
	6.8689	6.9263	0.0574		7.1298	7.1289	0.0009
O′	7.1689	7.2361	0.0672	O′	7.1938	7.1772	−0.0166
H	0.4245	0.3162	−0.1083	H	0.4009	0.3713	−0.0296
	0.4066	0.3809	−0.0257		0.4053	0.3843	−0.0210
H_2O	8	7.9332	−0.0668	H_2O	8	7.9328	−0.0672

https://doi.org/10.1021/acsomega.3c02686
ACS Omega 2023, 8, 28448−28455

doping, indicating that Fe doping could inhibit the electron transfer between the surface and H_2O molecule. Thus, the further poisoning reaction between H_2O and La_2CoFeO_6 is hindered, which proves that Fe doping has a significant effect on water poisoning resistance of perovskite catalyst.

4. CONCLUSIONS

The first-principles method based on DFT was used to calculate the adsorption properties of $LaCoO_3$ and La_2CoFeO_6. Through calculation and analysis of adsorption energy, Bader charge, and differential charge density, the following conclusions are obtained:

1. The poisoning mechanism of H_2O molecules in $LaCoO_3$ is that the H−O bond of H_2O is completely broken into hydroxyl and free hydrogen, and the free hydrogen combines with the surface oxygen to form a new hydroxyl group. The cycle is repeated, and the accumulation of a large number of hydroxyl groups on the catalyst surface prevents the activation of methane and oxygen on the catalyst surface.
2. When Fe is doped at the B-site, the H−O bond elongation of H_2O is weakened and the distance between H_2O and the surface is enlarged. The adsorption energy changes from −3.7493 eV on CoO_2 to −2.5397 eV on $CoFeO_4$, decreasing by about 1/3, indicating that Fe doping decreases the adsorption performance of water on the $CoFeO_4$ surface, making H_2O molecules not easily adsorbed on the $CoFeO_4$ surface.
3. The essence of H_2O adsorption on the surface is the transfer of electrons, and the amount of electron transfer is proportional to the adsorption energy. After doping the Fe element, the change of Bader charge on the surface of $CoFeO_4$ is reduced, and the ability to gain and lose electrons is weakened, which inhibits the adsorption of H_2O on the surface, and then inhibits the next toxic reaction. Compared with $LaCoO_3$, La_2CoFeO_6 has significantly enhanced water poisoning resistance, which provides a new idea for the research and design of perovskite catalyst materials.

AUTHOR INFORMATION

Corresponding Author

Xuefeng Wang − *College of Safety and Emergency Management Engineering, Taiyuan University of Technology, Taiyuan 030024 Shanxi, China*; orcid.org/0009-0005-0313-3460; Email: wxf6933@163.com

Authors

Cuihua Hao − *College of Safety and Emergency Management Engineering, Taiyuan University of Technology, Taiyuan 030024 Shanxi, China*

Shuangli Du − *College of Safety and Emergency Management Engineering, Taiyuan University of Technology, Taiyuan 030024 Shanxi, China*

Cunbao Deng − *College of Safety and Emergency Management Engineering, Taiyuan University of Technology, Taiyuan 030024 Shanxi, China*

Huijie Hu − *College of Safety and Emergency Management Engineering, Taiyuan University of Technology, Taiyuan 030024 Shanxi, China*

Complete contact information is available at: https://pubs.acs.org/10.1021/acsomega.3c02686

Author Contributions

Cuihua Hao: methodology, writing, and editing. **Xuefeng Wang:** investigation, visualization, and conceptualization. **Shuangli Du:** investigation, review, and conceptualization. **Cunbao Deng:** investigation and supervision. **Huijie Hu:** searching references.

Notes

The authors declare no competing financial interest.

ACKNOWLEDGMENTS

This work was supported by the National Natural Science Foundation of China (NSFC) (grant no. 51774172) and the Joint Funds of the NSFC-DFG (grant no. U1810206).

REFERENCES

(1) Omer, A. M. Energy, environment and sustainable development. *Renewable Sustainable Energy Rev.* **2008**, *12*, 2265−2300.

(2) Dorian, J. P.; Franssen, H. T.; Simbeck, D. R. Global challenges in energy. *Energy Policy* **2006**, *34*, 1984−1991.

(3) Yuan, J. The future of coal in China. *Resour., Conserv. Recycl.* **2018**, *129*, 290−292. (3a) Powell, J. B. Natural gas utilization: Current status and opportunities. *Catal. Today* **2020**, *356*, 27−36.

(4) Farquharson, D. V.; Jaramillo, P.; Schivley, G.; Klima, K.; Carlson, D.; Samaras, C. Beyond Global Warming Potential: A Comparative Application of Climate Impact Metrics for the Life Cycle Assessment of Coal and Natural Gas Based Electricity: Beyond Global Warming Potential. *J. Ind. Ecol.* **2017**, *21*, 857−873.

(5) Mann, R. Another Day Older and Deeper in Debt: How Tax Incentives Encourage Burning Coal and the Consequences for Global Warming[J]. *Pac. McGeorge Global Bus. & Dev. LJ* **2007**, *20*, 111.

(6) Herndon, J. M. Air Pollution, Not Greenhouse Gases: The Principal Cause of Global Warming. *J. Geog. Environ. Earth. Sci. Intn.* **2018**, *17*, 1−8.

(7) Edwards, G. A. S. Coal and climate change[J]. *Wiley Interdiscip. Rev. Clim. Change* **2019**, *10*, No. e607.

(8) Mallapaty, S. How China could be carbon neutral by mid-century. *Nature* **2020**, *586*, 482−483.

(9) Suda, T.; Fujii, M.; Yoshida, K.; Iijima, M.; Seto, T.; Mitsuoka, S. Development of flue gas carbon dioxide recovery technology. *Energy Convers. Manage.* **1992**, *33*, 317−324.

(10) Stasiulaitiene, I.; Martuzevicius, D.; Abromaitis, V.; Tichonovas, M.; Baltrusaitis, J.; Brandenburg, R.; Pawelec, A.; Schwock, A. Comparative life cycle assessment of plasma-based and traditional exhaust gas treatment technologies. *J. Cleaner Prod.* **2016**, *112*, 1804−1812.

(11) Tan, P.; Wang, D.; Lou, D.; et al. Progress of control technologies on exhaust emissions for agricultural machinery[J]. *Trans. Chin. Soc. Agric. Eng.* **2018**, *34*, 1−14.

(12) Deng, J.; Liu, Y.; Zhang, L.; et al. Advancements in catalysts for catalytic combustion of natural gas[J]. *Petrochem. Technol.* **2013**, *42*, 125−133.

(13) Zhuang, Q.; Melack, J. M.; Zimov, S.; Walter, K. M.; Butenhoff, C. L.; Khalil, M. A. K. Global Methan Emissions From Wetlands, Rice Paddies, and Lakes. *Eos, Transactions American Geophysical Union* **2009**, *90*, 37−38.

(14) Su, Y. S.; Ying, J. Y.; Green, W. H. Upper bound on the yield for oxidative coupling of methane. *J. Catal.* **2003**, *218*, 321−333.

(15) Deng, J.; Ren, P.; Deng, D.; Yu, L.; Yang, F.; Bao, X. Highly active and durable non-precious-metal catalysts encapsulated in carbon nanotubes for hydrogen evolution reaction. *Energy Environ. Sci.* **2014**, *7*, 1919−1923.

(16) Muroi, T. *Role of precious metal catalysts[J]*; Noble Metals, 2012; pp 301−334.

(17) Wang, J.; Gao, Y.; Kong, H.; Kim, J.; Choi, S.; Ciucci, F.; Hao, Y.; Yang, S.; Shao, Z.; Lim, J. Non-precious-metal catalysts for alkaline

water electrolysis: *operando* characterizations, theoretical calculations, and recent advances. *Chem. Soc. Rev.* **2020**, *49*, 9154−9196.
(18) Tanaka, H.; Misono, M. Advances in designing perovskite catalysts. *Curr. Opin. Solid State Mater. Sci.* **2001**, *5*, 381−387.
(19) Bian, Z.; Wang, Z.; Jiang, B.; Hongmanorom, P.; Zhong, W.; Kawi, S. A review on perovskite catalysts for reforming of methane to hydrogen production. *Renewable Sustainable Energy Rev.* **2020**, *134*, 110291.
(20) Misono, M. Recent progress in the practical applications of heteropolyacid and perovskite catalysts: Catalytic technology for the sustainable society. *Catal. Today* **2009**, *144*, 285−291.
(21) Madi, M.; Tahir, M. Highly stable $LaCoO_3$ perovskite supported g-C3N4 nanotextures with proficient charges migration for visible light CO_2 photoreduction to CO and CH4[J]. *Mater. Sci. Semicond. Process.* **2022**, *142*, 106517.
(22) Gu, J.; Zong, X.; Gao, A.; et al. Inactivation of CO sulfur-resistant Methanation catalyst MoS_2/Si-ZrO_2[J]. *CIESC J.* **2019**, *70*, 3941−3948.
(23) Cullis, C. F.; Nevell, T. G.; Trimm, D. L. Role of the catalyst support in the oxidation of methane over palladium. *J. Chem. Soc., Faraday Trans. 1* **1972**, *68*, 1406−1412.
(24) Zhang, F.; Hakanoglu, C.; Hinojosa, J. A.; Weaver, J. F. Inhibition of methane adsorption on PdO(101) by water and molecular oxygen. *Surf. Sci.* **2013**, *617*, 249−255.
(25) Li, X.; Wang, X.; Roy, K.; van Bokhoven, J. A.; Artiglia, L. Role of Water on the Structure of Palladium for Complete Oxidation of Methane. *ACS Catal.* **2020**, *10*, 5783−5792.
(26) Monteiro, R. S.; Zemlyanov, D.; Storey, J. M.; Ribeiro, F. Turnover Rate and Reaction Orders for the Complete Oxidation of Methane on a Palladium Foil in Excess Dioxygen. *Catal* **2001**, *199*, 291−301.
(27) Burch, R.; Urbano, F. J.; Loader, P. K. Methane combustion over palladium catalysts: The effect of carbon dioxide and water on activity. *Appl. Catal., A* **1995**, *123*, 173−184.
(28) Persson, K.; Pfefferle, L. D.; Schwartz, W.; Ersson, A.; Järås, S. G. Stability of palladium-based catalysts during catalytic combustion of methane: The influence of water. *Appl. Catal., B* **2007**, *74*, 242−250.
(29) Huang, Z.; Zhu, Z.; Liu, Z. Effect of V_2O_5/AC catalyst on low temperature reduction of NO[J]. *Chin. J. Catal.* **2001**, *22*, 532−536.
(30) Li, Z.; Chen, L.; Xie, C.; et al. Effect of water in reaction gas on performance of Molybdenum based methanation catalyst[J]. *J. Fuel Chem. Technol.* **2017**, *45*, 689−696.
(31) Yu, X.; Wang, L.; Chen, M.; Fan, X.; Zhao, Z.; Cheng, K.; Chen, Y.; Sojka, Z.; Wei, Y.; Liu, J. Enhanced activity and sulfur resistance for soot combustion on three-dimensionally ordered macroporous-mesoporous $Mn_xCe_{1-x}O_\delta/SiO_2$ catalysts[J]. *Appl. Catal., B* **2019**, *254*, 246−259.
(32) Hafner, J. *Ab-initio*simulations of materials using VASP: Density-functional theory and beyond. *J. Comput. Chem.* **2008**, *29*, 2044−2078.
(33) Wang, H. Q. Fundamental applications of Materials Studio software in molecular mechanics[J]. *Sci. Technol. Inf.* **2019**, *17*, 17−18.
(34) Constantin, L. A.; Perdew, J. P.; Tao, J. Meta-generalized gradient approximation for the exchange-correlation hole with an application to the jellium surface energy[J]. *Phys. Rev. B* **2006**, *73*, 205104.
(35) Tompsett, D. A.; Parker, S. C.; Bruce, P. G.; Islam, M. S. Nanostructuring of β-MnO_2: The Important Role of Surface to Bulk Ion Migration. *Chem. Mater.* **2013**, *25*, 536−541.
(36) Crespo, Y.; Seriani, N. A lithium peroxide precursor on the α-MnO_2(100) surface. *J. Mater. Chem. A* **2014**, *2*, 16538−16546.
(37) Crespo, Y.; Seriani, N. Electronic and Magnetic Properties of α-MnO2 from Ab Initio Calculations. *Phys. Rev. B* **2013**, *88*, 144428.
(38) Xuefeng, W.; Cuihua, H.; Shuangli, D.; Cunbao, D. Density functional theory of SO3 adsorption on the La2CoFeO6(001) surface. *Fuel* **2023**, *333*, 126489.

https://doi.org/10.1021/acsomega.3c02686
ACS Omega 2023, 8, 28448−28455